*Progress In Electromagnetics Research B, Vol. 46, 233–250, 2013*

# SIMULATION OF THE BEARING VOLTAGE IN AN INVERTER-FED INDUCTION MOTOR BY A FULL THREE PHASE MULTI CONDUCTOR TRANSMISSION LINE MODEL

**Biagio De Vivo[1, *], Patrizia Lamberti[1], Vincenzo Tucci[1], and Carlo Petrarca[2]**

[1]Department of Electronic and Computing Engineering, University of Salerno, Salerno 84084, Italy

[2]Department of Electrical Engineering, University of Naples Federico II, Naples 80125, Italy

**Abstract**—An accurate numerical model, based on multiconductor transmission lines (MTL) able to evaluate the voltage dynamics across the motor bearings and associated currents of an inverter-fed motor is presented. A full three phase stator winding of the wound type of a high power traction motor is considered in the proposed analysis. The different regions of the motor are modeled as suitable connections of lossy MTL which are then studied in the time domain. The per unit length characteristic matrices describing the MTL are accurately calculated by a FEM based software. The effects of the rise time of the input voltage and the length of the feeder cables are discussed. The reliability of the numerical results achieved by means of the MTL model is checked by performing a comparison with those obtained by considering a lumped parameter equivalent circuit.

## 1. INTRODUCTION

### 1.1. Bearing Voltage: State of Art

A drive system composed of a traditional induction motor matched to a pulse-width modulated (PWM) inverter can overcome the limitations of induction motors operating directly on line voltage, allowing an efficient control of the ac-motor speed by varying the amplitude and frequency of the supply voltage, thus obtaining an adjustable-speed

*Received 6 September 2012, Accepted 23 November 2012, Scheduled 30 November 2012*
Corresponding author: Biagio De Vivo (bdevivo@unisa.it).

drive (ASD). One of the most common techniques adopted for the generation of the desired output voltage waveforms is PWM which has reached great diffusion thanks to the rapid development of new switching devices, such as the insulated gate bipolar transistor (IGBT), which can reach high switching frequencies with low power losses.

Unfortunately, the output voltage from the inverter is not purely sinusoidal and, in particular, steep front pulses can be generated in correspondence to the commutations of the IGBTs, resulting in a high frequency (HF) common mode voltage (CMV) at the motor terminals. Such CMV determines intense electrical stresses, very dissimilar from those observed when feeding the motor with a pure sinusoidal waveform, which, in turn, may influence the performances of various parts of the motor, such as the motor insulation and the bearings. In particular, the motor electrical insulation experiences high turn-to-turn stress caused by non-uniform potential distributions, increased dielectric heating, intense partial discharge (PD) activity due to overshoots in pulse waveforms and space charge accumulation which in different way affect the material life time [1–8].

Furthermore, the mismatch among the impedances of inverter, cable and motor induces different types of bearing currents (BC) which may determine early aging and possible failure of such critical components. A very ample literature is available on the physical mechanisms of the failure, the modeling approaches and the possible mitigation techniques of such parasitic currents. In particular, a very interesting paper has been recently proposed by Muetze in which the different contributions proposed so far on such different aspects have been thoroughly reviewed [9]. Muetze and Binder have also provided a clear classification of the different mechanisms responsible of BC as well as significant results from experimental tests [10–16]. Among the different BC mechanisms, the so called circulating bearing currents flowing in the loop stator frame-nondrive end-shaft drive end of the motor may assume, depending on the motor size, very high peak values (up to 20 A for a 400 V, 500 kW machine) [10, 13]. Such currents are caused by a shaft voltage which, in turn, depends on the stator-winding-to-frame capacitance excited by the high dv/dt of the CMV.

### 1.2. Bearing Voltage: Prediction Models

For design purposes, it is of great importance to provide the electrical engineer with a model able to predict the voltage on the rotor shafts as a function of some relevant geometrical and electrical parameters, such as the stator dimension, the length of feeding cable, shape of the applied voltage, insulating material permittivity etc..

Most models available in the literature are based on a

representation of the motor winding as a lumped parameter network and cannot take into account the effects of wave propagation within a coil [11, 16, 17]. Other more accurate approaches [18, 19] adopt a multiconductor transmission lines (MTL) model which allows to take into account the spatial distribution of the voltage inside the system, but are not intended for providing information on the bearing currents.

For this reason, based on an MTL model [20] which takes into consideration also the frequency dependent joule losses, the authors have developed a MTL model of the motor winding, able to predict the voltages across the rotor shaft and to estimate the currents flowing through the bearings when the machine is fed by a single-phase ramp voltage with variable slew rate [21, 22].

In the previous paper [21] the MTL model considered a single phase of a motor, in the present paper the MTL model is extended to the full three phase stator winding of a traction motor in order to take into account the effects of a typical three-phase inverter output voltage. The MTL line is studied in the time-domain by using the telegraphers' equation system with suitable boundary conditions. This mathematical model leads to a set of equations representing an equivalent circuit given by a $2n$-port. The model can properly take into account the presence of Joule losses along the line, together with the skin effect. However, in order to reduce the computation time and the memory requirements, resistive lumped parameters $R$ have been considered at the junctions between two adjacent MTL. The per unit length characteristic matrices describing the line have been accurately calculated by a FEM based software.

The paper is organized as follows. After a short description of the adopted model and the solution technique, results about the evaluation of the voltage across the bearings and on the effects of the rise time of the input voltage, the length of the feeder cables are discussed. The reliability of the numerical results achieved by means of the MTL model is checked by performing a comparison with those obtained by considering a lumped parameter equivalent circuit.

## 2. THE CONSIDERED MODEL

### 2.1. MTL Model of the Motor

In Figure 1 a typical stator coil of a traction motor of the wound type is shown. It can be split into 6 sections (T1 ... T6) where (T2, T5) represent the conductors in the slots, and the remaining sections (T1, T6) and (T3, T4) stand for the conductors in the overhang regions, and $N$ is the number of conductors per slot in each stator winding.

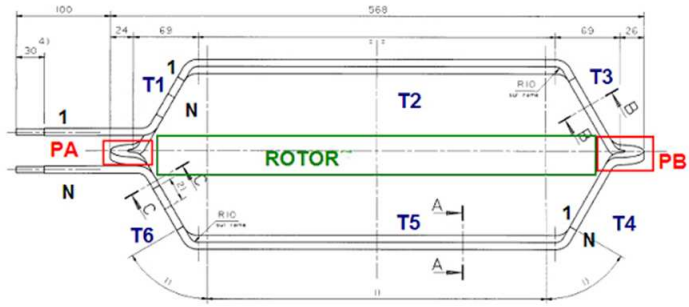


**Figure 1.** Typical stator coil of a form wound motor. The different sections considered in the proposed model are evidenced.

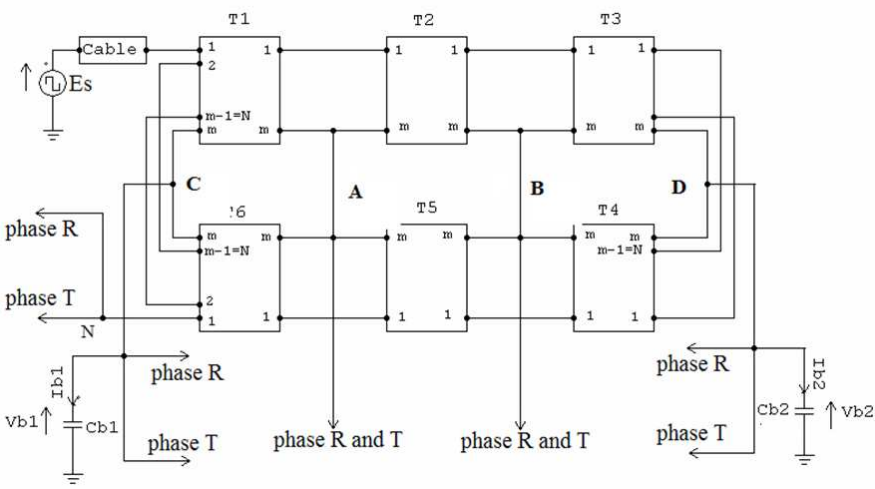


**Figure 2.** The MTL model (phase $S$) associated to the considered inverter drive.

In the hypothesis that the field structure is Transverse ElectroMagnetic (TEM) or quasi-TEM the voltage distribution across the coil can be calculated by using the MTL theory and the telegrapher's equations.

The electrical model is composed of a connection of 6 MTL per electrical phase ($R$, $S$, $T$); each MTL is represented by $N + 1$ conductors, where $N$, as mentioned before, is the numbers of conductors per slot in each stator winding and the last conductor represents the rotor which is common to all the three phases (Figure 2).

At its ends, the rotor is connected to a pair of bearings represented in the picture by their equivalent capacitance $C_{b1}$ and $C_{b2}$. The presence of the feeder cable, connecting the inverter to the motor, is taken into account by means of a single transmission line per phase.

The MTLs are described by their characteristic $\underline{\underline{\mathbf{R}}}$, $\underline{\underline{\mathbf{L}}}$, $\underline{\underline{\mathbf{C}}}$, $\underline{\underline{\mathbf{G}}}$ per unit length (p.u.l.) matrices, and in particular, the matrix $\underline{\underline{\mathbf{G}}}$ represents the dielectric losses in the windings, $\underline{\underline{\mathbf{R}}}$ is associated to the losses in

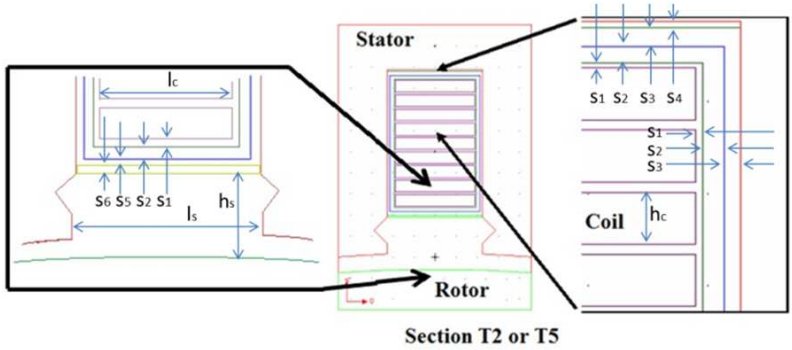


**Figure 3.** Transverse section of the T2 or T5 stator domain. The dimensions adopted for the computation of the parameters of the MTL matrices are indicated.

**Table 1.** Geometrical parameters (see Figure 3) adopted in the FEM computations for the considered motor. The values of the relative permittivity of the different insulating materials are also reported.

| Parameter | Name | Value (mm) | $\varepsilon_r$ |
|---|---|---|---|
| conductor insulation | $S_1$ | 0.11 | 3.4 |
| coil insulation | $S_2$ | 0.36 | 6 |
| groundwall insulation | $S_3$ | 0.26 | 3.4 |
| bottom slot spacer | $S_4$ | 0.13 | 3.6 |
| additional insulation | $S_5$ | 0.42 | 3.4 |
| top slot spacer | $S_6$ | 0.13 | 2.4 |
| slot to rotor distance | $h_s$ | 4.97 | 1 |
| slot width | $l_s$ | 9.07 | 1 |
| height of conductor cross section | $h_c$ | 1.13 | |
| length of conductor cross section | $l_c$ | 7.58 | |
| rotor radius | $r_r$ | 140 | |
| stator radius | $r_s$ | 138.5 | |

the windings, $\underline{\underline{\mathbf{L}}}$ and $\underline{\underline{\mathbf{C}}}$, are respectively the matrices of the inductance and capacitance of the windings.

In Figure 3 a transverse section of the T2 or T5 domain adopted for the computation of the p.u.l. matrix is depicted. The number of conductors per slot in each stator winding is equal to 9, leading to $[10\times10]$ $\underline{\underline{\mathbf{L}}}$ and $\underline{\underline{\mathbf{C}}}$ matrices. The parameters of such matrices have been accurately calculated by a commercial software (Maxwell® by Ansoft Co) based on the finite element method (FEM) [23]. The values of the geometrical and physical quantities adopted in the computations are given in Table 1, this values are obtained from the layout and data-sheet of a typical traction motor with nominal power of 373 kW. The same procedure has been applied to determine the matrices elements of all the different domains composing the winding.

In the Laplace domain it is possible to obtain the longitudinal impedance $\underline{\underline{\mathbf{Z}}}(s) = \underline{\underline{\mathbf{R}}} + s\underline{\underline{\mathbf{L}}}$ and transverse admittance $\underline{\underline{\mathbf{Y}}}(s) = \underline{\underline{\mathbf{G}}} + \mathbf{s}\underline{\underline{\mathbf{C}}}$. The MTL line is studied in the time-domain by means of the $2n$-port model depicted in Figure 4 and described by (1) and (2)

$$\begin{cases} \underline{\mathbf{i}}_0(t) = \int_{0^-}^{t+} \underline{\underline{\mathbf{Y}}}_c(t-\tau) \times \underline{\mathbf{v}}_0(\tau)d\tau + \underline{\mathbf{j}}_0(t) \\ \underline{\mathbf{i}}_d(t) = \int_{0^-}^{t+} \underline{\underline{\mathbf{Y}}}_c(t-\tau) \times \underline{\mathbf{v}}_d(\tau)d\tau + \underline{\mathbf{j}}_d(t) \end{cases} \tag{1}$$

with

$$\begin{cases} \underline{\mathbf{j}}_0(t) = \int_{0^-}^{t+} \underline{\underline{\mathbf{P}}}(t-\tau) \times \left[-2\underline{\mathbf{i}}_d(\tau) + \mathbf{j}_d(\tau)\right] d\tau \\ \underline{\mathbf{j}}_d(t) = \int_{0^-}^{t+} \underline{\underline{\mathbf{P}}}(t-\tau) \times \left[-2\underline{\mathbf{i}}_0(\tau) + \mathbf{j}_0(\tau)\right] d\tau \end{cases} \tag{2}$$

The different quantities appearing in (1), (2) are indicated on the scheme in Figure 4. The $\{\underline{\mathbf{i}}_0(t), \underline{\mathbf{v}}_0(t)\}$ and $\{\underline{\mathbf{i}}_d(t), \underline{\mathbf{v}}_d(t)\}$ are respectively, the current and the voltage at the input and output of the $2n$-port model shown in Figure 4. The matrices $\underline{\underline{\mathbf{Y}}}_c(t)$ and $\underline{\underline{\mathbf{P}}}(t)$ are, respectively, the Laplace transform of the characteristic admittance $\underline{\underline{\mathbf{Y}}}_c(s) = \sqrt{\underline{\underline{\mathbf{Z}}}^{-1}(s) \times \underline{\underline{\mathbf{Y}}}^{-1}(s)} \times \mathbf{Y}(s)$ and of the propagation function

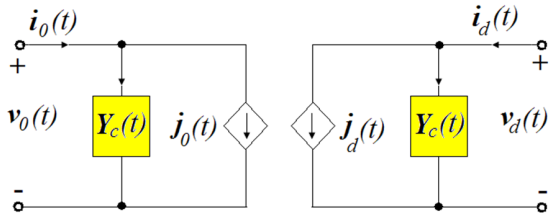


**Figure 4.** $2n$-port model of the MTL.

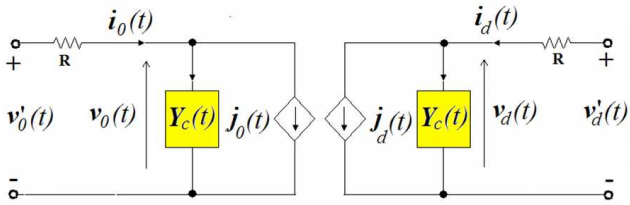


**Figure 5.** Modified $2n$-port with concentrated elements $R$ which account for winding losses.

$\underline{\underline{\mathbf{P}}}(s) = \exp(d \times \sqrt{\underline{\underline{\mathbf{Z}}}(s)\underline{\underline{\mathbf{Y}}}(s)})$. Details on the model and the solution technique can be found in [18]. The solution can be achieved by means of a recursive approach since at time instant $t$ the state variables $\underline{\mathbf{j}}_0(t)$ and $\underline{\mathbf{j}}_d(t)$ are known because they depend on the values assumed by themselves and by the currents at time instant $(t-T)$, where $T$ is the propagation time delay.

In order to decrease the computational burden (in terms of computing time and memory usage) the following approximations are considered $\underline{\underline{\mathbf{G}}} = 0$, i.e., no losses in the dielectric materials, whereas the losses in the windings are considered as two concentrated elements at the input and output of the $2n$-port. As a consequence, the circuit of Figure 4 is changed into that shown in Figure 5, whereas the system of equations to be solved becomes:

$$\begin{cases} \left(\underline{\underline{\mathbf{I}}} + \underline{\underline{\mathbf{RY}}}\right) \times \underline{\mathbf{i}}_0(t) - \underline{\underline{\mathbf{Y}}} \times \underline{\mathbf{v}}_d(t) = \underline{\mathbf{j}}_0(t) \\ \left(\underline{\underline{\mathbf{I}}} + \underline{\underline{\mathbf{RY}}}\right) \times \underline{\mathbf{i}}_d(t) - \underline{\underline{\mathbf{Y}}} \times \underline{\mathbf{v}}_d(t) = \underline{\mathbf{j}}_d(t) \end{cases} \tag{3}$$

To solve the circuit of Figure 5, for each section the appropriate systems (2) and (3) must be solved in the time domain together with $3 \times M \times 2 \times m$ matching conditions, where $M$ is the number of MTL and $m$ is the number of conductors in each MTL. For example, the systems of equations to be considered at the interface between Sections 3 and 4 of Figure 1 at the time instant $t_k$ is:

$$\begin{cases} v_0'(T_{3S}, i, t_k) - v_d'(T_{4S}, i+1, t_k) = 0 \\ v_0'(T_{3R}, i, t_k) - v_d'(T_{4R}, i+1, t_k) = 0 \quad \text{with} \quad i = 1, \ldots, m-1 \\ v_0'(T_{3T}, i, t_k) - v_d'(T_{4T}, i+1, t_k) = 0 \\ v_d'(T_{3S}, m, t_k) = v_d'(T_{3R}, m, t_k) = v_d'(T_{3T}, m, t_k) = v_{b2}(t_k) \\ v_0'(T_{4S}, 1, t_k) = v_0'(T_{4R}, 1, t_k) = v_0'(T_{4T}, 1, t_k) = v_{b2}(t_k) \end{cases} \tag{4}$$

$$\begin{cases} i_0\left(T_{4S}, i+1, t_k\right) + i_d\left(T_{3S}, i, t_k\right) = 0 \\ i_0\left(T_{4R}, i+1, t_k\right) + i_d\left(T_{3R}, i, t_k\right) = 0 \quad \text{with} \quad i = 1, \ldots, m \\ i_0\left(T_{4T}, i+1, t_k\right) + i_d\left(T_{3T}, i, t_k\right) = 0 \\ i_0\left(T_{4S}, 1, t_k\right) + i_d\left(T_{3S}, m, t_k\right) + i_0\left(T_{4R}, 1, t_k\right) + i_d\left(T_{3R}, m, t_k\right) \\ + i_0\left(T_{4T}, 1, t_k\right) + i_d\left(T_{3T}, m, t_k\right) + i_{b2}(t_k) = 0 \\ i_{b2}\left(t_k\right) = C_{b2}\left[v_{b2}(t_k) - v_{b2}(t_{k-1})\right]/\Delta \end{cases} \tag{5}$$

where the suffixes ($R$, $S$, $T$) concern the three phases of the motor and $\Delta$ is the time interval adopted for the integration ($\Delta = t_k - t_{k-1}$). It is worth noting that at the analyzed interface also the bearing capacitance $C_b$ is considered.

## 2.2. Model of the Cable

The cable connecting the inverter with the motor is modeled by a lumped parameters $\pi$ network as shown in Figure 6. The network parameters are:

$$\begin{cases} R_S = d_c \times r_{\text{pul}} \\ L_S = d_c \times l_{\text{pul}} \\ R_p = d_c \times \frac{1}{g_{\text{pul}}} \\ c_p = d_c \times c_{\text{pul}} \end{cases} \tag{6}$$

where $d_c$ is the length of the cable, and $r_{\text{pul}}$, $l_{\text{pul}}$, $g_{\text{pul}}$ and $c_{\text{pul}}$ are respectively the p.u.l. series resistance, series inductance, parallel conductance and parallel capacitance.

The variables $v_0'(1,t)$ and $i_0(1,t)$ reported on Figure 6 are related to voltage and input current of the first conductor concerning the section T1 of the MTL network. The relation between $v_0'(1,t_k)$ and $i_0(1,t_k)$ and the voltage and current delivered by the generator is given by the system:

$$\begin{cases} \left(\frac{1}{R_g} + \frac{c_p}{2\Delta} + \frac{c_g}{2}\right) v_1\left(t_k\right) + i_2\left(t_k\right) = \frac{E_g(t_k)}{R_g} + \frac{c_p}{2\Delta} v_1\left(t_{k-1}\right) \\ v_0'\left(1, t_k\right) - v_1\left(t_k\right) + \left(R_S + \frac{L_S}{\Delta}\right) i_2\left(t_k\right) = \frac{L_S}{\Delta} i_2\left(t_{k-1}\right) \\ \left(\frac{c_p}{2\Delta} + \frac{c_g}{2}\right) v_0'\left(1, t_k\right) + i_0\left(1, t_k\right) - i_2\left(t_k\right) = \frac{c_p}{2\Delta} v_0'\left(1, t_{k-1}\right) \end{cases} \tag{7}$$

where $v_0'(1,t_{k-1})$ and $i_0(1,t_{k-1})$ are the voltage and current, respectively, to the MTL input to time $t_{k-1}$. In order to solve the circuit of Figure 2, 720 equations for each of the system (2), (3) and (5), (6) are to be written together with 9 equations (7) for the three power supply cables (one for each phase).

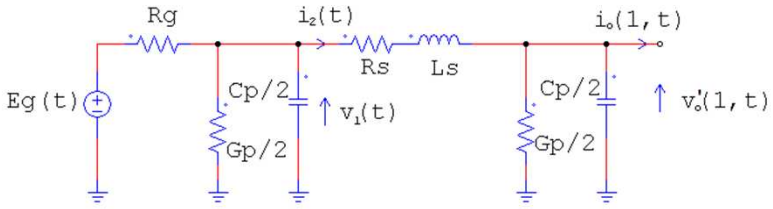


**Figure 6.** $\pi$ model of the cable.

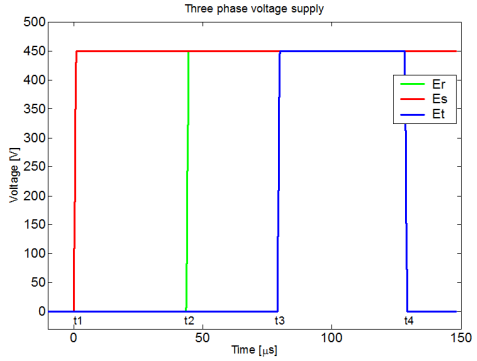


**Figure 7.** Supply voltages adopted in the simulations.

## 3. NUMERICAL RESULTS

The traction motor used for the simulation has a form wound stator coil characterized by 9 conductors per slot. The considered circuital model includes 6 MTL per phase, each one composed of 10 lines. Each motor phase is connected through a feeder cable to an ideal voltage supply.The power voltage reproduces a typical three-phase inverter output, as shown in Figure 7.

A characteristic time interval of 150 µs has been chosen for the simulations, since at time instants $t_1$, $t_2$ and $t_3$ for each phase $S$, $R$, $T$, respectively, a step up can be found, while only one step down (at $t = t_4$) for phase $T$ occurs. The output voltage for each phase has a maximum value of 450 V and is characterized by its slew rate $d\,(\mathrm{dV/dt})$.

Figure 8 shows the plots of the time behavior of the voltage $V_{b1}$ and $V_{b2}$ (a) and current $I_{b1}$, $I_{b2}$ (b) on the two bearings, obtained on the basis of simulations performed by considering typical values of the parameters of a traction machine, i.e., the length of the power cable

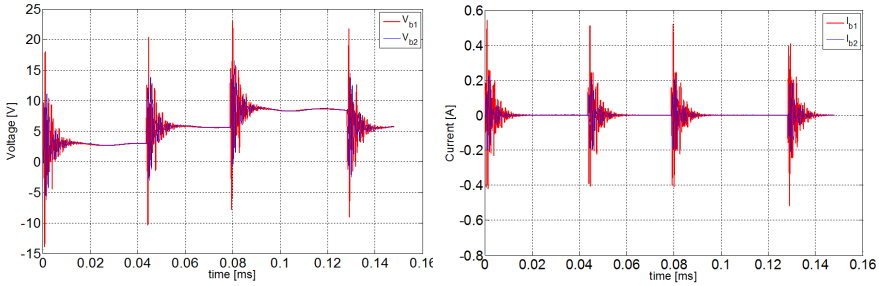


**Figure 8.** Time evolution of the (a) voltages $V_{b1}$ and $V_{b2}$ and (b) currents $I_{b1}$, $I_{b2}$ on the two bearings for the applied voltages of Figure 7.

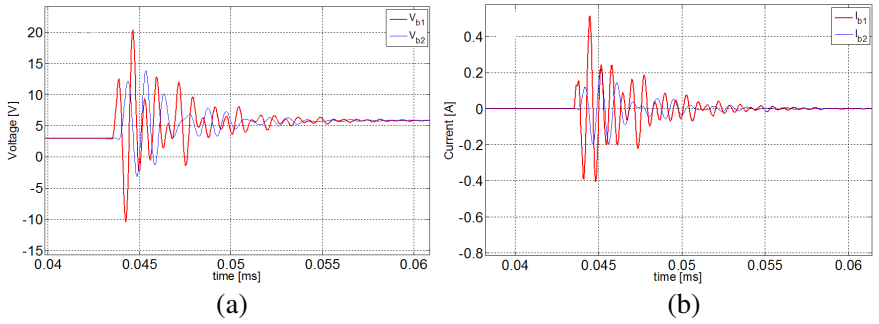


**Figure 9.** Zoom of the (a) voltages $V_{b1}$ and $V_{b2}$ and (b) currents $I_{b1}$, $I_{b2}$ on the two bearings occurring at the instant $t_2$.

($d_c$) equal to 5 meters, the slew rate ($d$) 1.5 kV/µs and the length $s$ of the sections T2 and T5 equal to 0.38 m. It is evident from Figure 8 that both the voltage and the current in the two bearings are different and the difference is correlated to the commutation of the switching devices.

A clearer view of the differences can be noted from the plots in Figure 9 where a zoom of the current and voltage waveforms is reported for a time interval around the instant $t_2$ where the commutation of phase $S$ occurs.

The signal on the second bearing (blue color lines in Figures 8 and 9) starts with a delay with respect to that on the first one.

Moreover, the maximum values reached by both the voltage and current on the first bearing (red color lines in Figures 8 and 9) are greater than those on the second one.

From this observation it is confirmed that the drive-end bearing is the most stressed and therefore it is the one that requires more attention in the design phase.

### 3.1. Effect of the Slew Rate $d$

In order to evaluate the influence of the slew rate of the applied voltage three values have been considered in the simulations, $d = [0.5,\ 1.5,\ 3.0]\,\mathrm{kV/\mu s}$.

In Figure 10 the time evolution of the voltages $V_{b1}$ and $V_{b2}$ (a) and the current $I_{b1}$ and $I_{b2}$ (b) across the two bearings, for $d = 0.5\,\mathrm{kV/\mu s}$ and $d = 3.0\,\mathrm{kV/\mu s}$, are shown. It can be noted that the slew rate, as expected, has a significant impact on the two considered quantities.

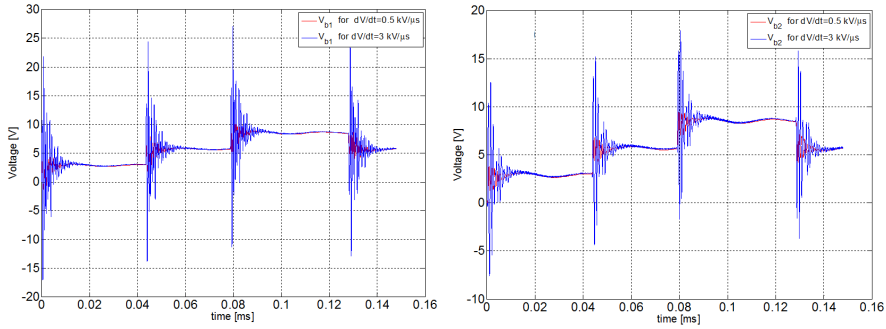


**Figure 10.** Time evolution of (a) $V_{b1}$ and (b) $V_{b2}$ across the bearings with the slew rate as a parameter.

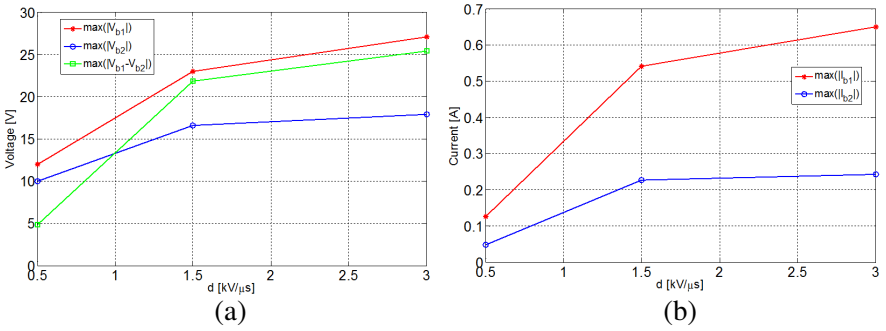


**Figure 11.** Max values of (a) $|V_{b1}|$, $|V_{b2}|$ and $|V_{b1} - V_{b2}|$ and (b) $|I_{b1}|$ e $|I_{b2}|$, as a function of the slew rate.

In Figure 11 the max value of the two bearing voltages and currents together with the absolute value of their difference is reported as a function of the slew rate when the motor is connected through a 5 m feeding cable to the inverter.

It is clearly evident that the maximum voltage is obtained for the greatest value of $d$ and the effect is more marked for the drive-end bearing. Instantaneous values of about 25 V can be obtained for the max voltage difference.

It is worth observing that such difference is not necessarily obtained for the same conditions leading to the max for $V_{b1}$ and $V_{b2}$.

### 3.2. Effect of Cable Length $d_c$

Three different lengths of the cable connecting the inverter to the motor have been considered, $d_c = [2,\ 5,\ 30]$ m. The voltages across

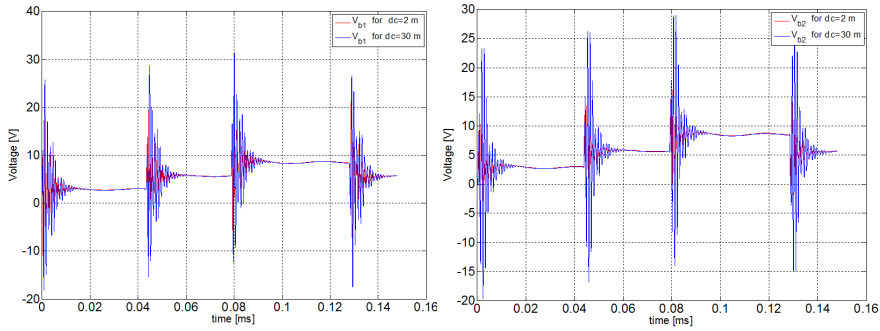


**Figure 12.** Time evolution of (a) $V_{b1}$ and (b) $V_{b2}$ across the bearings with the cable length as a parameter.

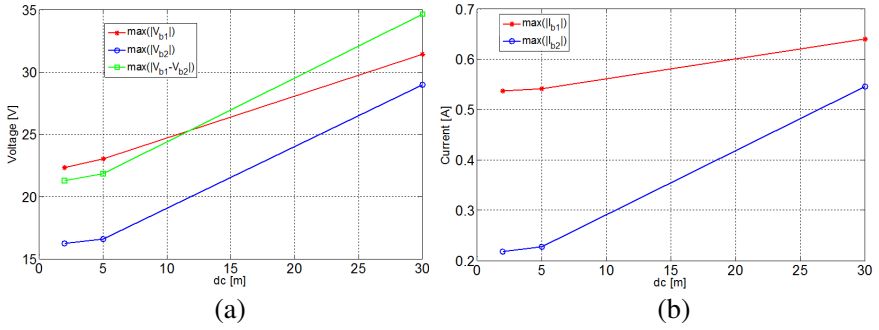


**Figure 13.** Max values of (a) $|V_{b1}|$, $|V_{b2}|$ and $|V_{b1} - V_{b2}|$ and (b) $|I_{b1}|$ e $|I_{b2}|$, as a function of the cable length.

**Table 2.** Max values of $V_{b1}$ and $V_{b2}$ for different values of $d$ and $d_c$.

| | $d$ [kV/μs] | | | $d_c$ [m] | | |
|---|---|---|---|---|---|---|
| | 0.5 | 1.5 | 3.0 | 2 | 5 | 30 |
| $V_{b1}$ [V] | 12 | 23.8 | 27.1 | 22.3 | 23.4 | 31.4 |
| $V_{b2}$ [V] | 10 | 16.7 | 18 | 16.2 | 16.7 | 29.0 |

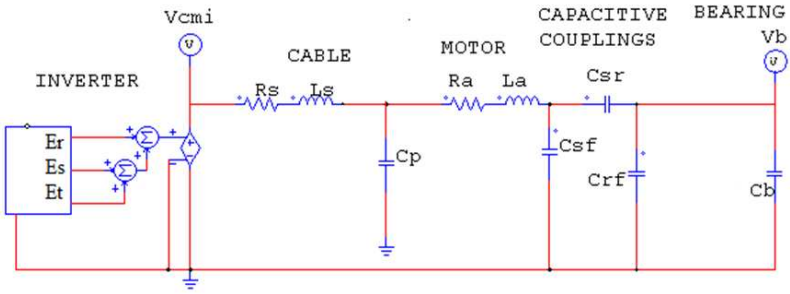


**Figure 14.** Lumped parameters equivalent circuit for the system of Figure 2.

the bearings have been calculated with $d = 1.5\,\text{kV/μs}$ and $s = 0.38\,\text{m}$. In Figures 12 and 13 the detrimental effect on the voltage distribution produced by longer cables is shown.

As shown in Table 2, the increase of rise time ($d$) has its major effect on the drive end bearing (bearing 1). In fact, by rising the slew rate from 0.5 kV/μs up to 3 kV/μs we get an over voltage $\Delta V$ on the two bearings which is, respectively, $\Delta V_{b1} = 15\,\text{V}$ and $\Delta V_{b2} = 8\,\text{V}$. Greater lengths of the feeding cable ($d_c$) cause higher stresses on the non drive end bearing (bearing 2). Indeed $\Delta V_{b1} = 9.1V$ e $\Delta V_{b2} = 12.8\,\text{V}$, when changing the connecting cable length from 2 m up to 30 m.

### 3.3. MTL Model vs. Lumped Parameter Circuit

As for most numerical models, an intrinsic drawback associated also to the MTL approach herein described, is the difficulty to assess the accuracy and reliability of the obtained results. Experimental verifications are evidently very complex, if not impossible. Therefore, in order to perform a validation (at least an indirect one) of the proposed model, the results achieved by means of the MTL model have

**Table 3.** Values of the components for the lumped parameter circuit of Figure 14.

| Parameter | Value | Description |
|---|---|---|
| $V_{\max}$ | 45 V | Maximum voltage |
| Freq_$m$ | 50 Hz | Output frequency |
| Freq_$p$ | 4000 Hz | Switching frequency |
| $d$ | 1.5 kV/μs | Output Slew Rate |
| $L_s$ | 0.53 mH | Longitudinal inductance of cable feeder |
| $R_s$ | 1.03 mΩ | Longitudinal resistance of cable feeder |
| $C_p$ | 2 nF | Transversal capacitance of cable feeder |
| $d_c$ | 5 m | Length of cable feeder |
| $R_a$ | 24.2 mΩ | Resistance of the stator coil |
| $L_a$ | 3.53 mH | Inductance of the stator coil |
| $C_{sf}$ | 3.45 nF | Capacitance between stator coli and frame |
| $C_{sr}$ | 17 pF | Capacitance between stator coli and rotor |
| $C_{rf}$ | 263 pF | Capacitance between rotor and frame |
| $C_b$ | 3 nF | Capacitance of the bearings |

been compared with those obtained by using the lumped-parameters equivalent model shown in Figure 14 [24], simulated with PSIM®. Such model has proved efficient in exploiting results comparable to experimental findings as it concerns the statistical indicators associated to the Electrical Discharge Machining (EDM) currents occurring in the bearings of inverter-driven ac motors [24, 25].

In Table 3 the values of the components of the circuit of Figure 14 are reported. Figure 15 shows the results of the simulations obtained by using the lumped parameter circuit together with those achieved by means of the MTL model. For the former circuit, in addition to the voltage on the bearing, the common-mode voltage of the inverter output $V_{cmi} = (E_S + E_R + E_T)/3$ [26] (such values are divided by 40 for graphic reasons) is also shown.

The comparison among the two simulation models concerns the voltage ($V_{st}$) at the end of the oscillating phase that arises in correspondence of the switching of one phase, the length of the swing phase ($\Delta t$) and the maximum amplitude of the voltage during the oscillating phase ($\Delta V$). For the case of the distributed parameter circuit two values of $\Delta t$ and $\Delta V$ are given, indicated by the subscripts 1 and 2, and corresponding to the two bearings $C_{b1}$ and $C_{b2}$. Such values are presented in Table 4, where for the lumped parameter circuit only one value can be evaluated.

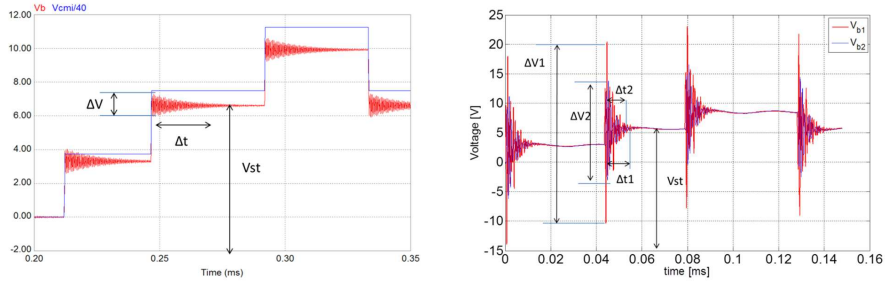


**Figure 15.** Comparison of the bearing voltages obtained with lumped and MTL models: (a) common mode voltage and bearing voltage simulated by means of the lumped circuit; (b) bearing voltage obtained by MTL model.

**Table 4.** Comparison of the characteristic quantities describing the voltage on the bearings as obtained from the MTL model and the lumped parameter circuit.

| | Lumped | MTL model ($C_{b1}$) | MTL model ($C_{b2}$) |
|---|---|---|---|
| $V_{st}$ (V) | 6.3 | 5.9 | 5.9 |
| $\Delta t$ (ms) | 0.027 | 0.0106 | 0.0084 |
| $\Delta V$ (V) | 1.5 | 29.5 | 18.3 |

From Table 4 it can be observed that both models lead to the same voltage $V_{st}$. In fact, this value depends on the Bearing Voltage Ratio (BVR) [24–28] and for both models such a parameter should be roughly the same. The slight difference is due to the resolution of two different software used for the circuits and how these capacities are calculated in the evaluation of the BVR. A remarkable difference is obtained for the values of $\Delta V$. This value is equal to 1.5 V for the lumped parameter circuit, but can be even 20 times higher for the MTL model. Such a difference, originated by the reflection phenomena, highlights that EDM currents, which in the lumped parameter model cannot be taken into account, may arise [24, 27].

## 4. CONCLUSION

The results obtained by simulations performed with a full three phase MTL model for a high power traction motor have been discussed. The elements of the per unit length characteristic matrices describing the

lines are calculated by a FEM based software, whereas resistive lumped parameters have been considered at the junctions between two adjacent MTL in order to take into account Joule losses. The MTL model allows to get an accurate evaluation of the critical quantities affecting the reliability of inverter-fed traction motors, such as the different voltage dynamics across the two motor bearings and the associated currents flowing through the bearings. The evaluation of such quantities cannot be achieved by considering lumped parameters network since they cannot take into account the propagation and reflection phenomena.

## REFERENCES

1. Bonnett, A. H., "Analysis of the impact of pulse-width modulated inverter voltage waveforms on AC induction motors," *IEEE Trans. on Industry Applications*, Vol. 32, 386–392, 1996.
2. Kaufhold, M., H. Auinger, M. Berth, J. Speck, and M. Eberhardt, "Electrical stress and failure mechanism of the winding insulation in PWM-inverter-fed low-voltage induction motors," *IEEE Trans. on Industrial Electronics*, Vol. 47, No. 2, 396–402, 2000.
3. Cavallini, A., D. Fabiani, and G. C. Montanari, "Power electronics and electrical insulation systems — Part 1: Phenomenology overview," *IEEE Electrical Insulation Magazine*, Vol. 26, No. 3, 7–15, 2010.
4. Melfi, M., A. M. J. Sung, S. Bell, and G. L. Skibinski, "Effect of surge voltage risetime on the insulation of low-voltage machines fed by PWM converters," *IEEE Trans. on Industry Applications*, Vol. 34, 766–775, 1998.
5. Lipo, T. A., G. Venkataramanan, and S. Bernet, "High-frequency modeling for cable and induction motor overvoltage studies in long cable drives," *IEEE Trans. on Industry Applications*, Vol. 38, No. 5, 1297–1306, 2002.
6. Lupò, G., C. Petrarca, V. Tucci, and M. Vitelli, "Multiconductor transmission line analysis of steep-front surges in machine windings," *IEEE Trans. on Dielectrics and Electrical Insulation*, Vol. 9, No. 3, 467–478, 2000.
7. Haq, S. U., S. H. Jayaram, and E. A. Cherney, "Evaluation of medium voltage enameled wire exposed to fast repetitive voltage pulses," *IEEE Trans. on Dielectrics and Electrical Insulation*, Vol. 14, No. 1, 194–203, 2007.
8. Zhang, P., Y. Du, T. G. Habetler, and B. Lu, "A survey of condition monitoring and protection methods for medium-voltage

induction motors," *IEEE Trans. on Industry Applications*, Vol. 47, No. 1, 34–46, 2011.

9. Muetze, A., "Thousands of hits: On inverter-induced bearing currents, related work, and the literature," *Elektrotechnik & Informationstechnik*, Vol. 128, No. 11–12, 382–388, 2011.
10. Muetze, A. and A. Binder, "Techniques for measurement of parameters related to inverter-induced bearing currents," *IEEE Trans. on Industry Applications*, Vol. 43, No. 5, 1274–1283, 2007.
11. Muetze, A. and A. Binder, "Scaling effects of inverter-induced bearing currents in AC machines," *IEEE Trans. on Industry Applications*, Vol. 44, No. 4, 965–972, 2008.
12. Muetze, A. and A. Binder, "Calculation of circulating bearing currents in machines of inverter-based drive systems," *IEEE Trans. on Industrial Electronics*, Vol. 54, No. 2, 932–938, 2007.
13. Muetze, A. and A. Binder, "Practical rules for assessment of inverter-induced bearing currents in inverter-fed AC motors up to 500 kW," *IEEE Trans. on Industrial Electronics*, Vol. 54, No. 3, 1614–1622, 2007.
14. Di Piazza, M. C., A. Ragusa, and G. Vitale, "Power-loss evaluation in CM active EMI filters for bearing current suppression," *IEEE Trans. on Industrial Electronics*, Vol. 58, No. 10, 5142–5143, 2011.
15. Ferreira, F. J. T., M. V. Cistelecan, and A. T. de Almeida, "Evaluation of slot-embedded partial electrostatic shield for high-frequency bearing current mitigation in inverter-fed induction motors," *IEEE Trans. on Energy Conversion*, Vol. 27, No. 2, 382–390, 2012.
16. Ahmed, A. S. and G. Skibinski, "Design and analysis of an integrated differential-common mode filter for on site motor bearing problems," *2011 IEEE International Electric Machines & Drives Conference (IEMDC)*, 283–289, 2011.
17. Naik, R., T. A. Nondhal, M. Melfi, R. Schiferl, and J. Wang, "Circuit model for shaft voltage prediction in induction motors fed by PWM-based AC drives," *IEEE Trans. on Industry Applications*, Vol. 39, No. 5, 1294–1299, 2003.
18. Wright, M. T., S. J. Yang, and K. McLealy, "General theory of fast-fronted interturn voltage distribution in electrical machine windings," *IEE Proceedings B — Electric Power Applications*, Vol. 130, 245–256, 1983.
19. Guardado, J. L., J. A. Flores, V. Venegas, J. L. Naredo, and F. A. Uribe, "A machine winding model for switching

transient studies using network synthesis," *IEEE Trans. on Energy Conversion*, Vol. 20, No. 2, 322–328, 2005.

20. Petrarca, C., A. Maffucci, V. Tucci, and M. Vitelli, "Analysis of the voltage distribution in a motor stator winding subjected to steep-fronted surge voltages by means of a multiconductorlossy transmission line model," *IEEE Trans. on Energy Conversion*, Vol. 19, No. 1, 7–17, 2004.
21. De Vivo, B., C. Petrarca, V. Tucci, and M. Vitelli, "A multi conductor transmission line model for the evaluation of the rotor shaft voltages in adjustable speed drive motors," *PIERS Proceedings*, 236–240, Cambridge, MA, USA, Mar. 26–29, 2006.
22. De Vivo, B., "Valutazione degli effetti prodotti dall'utilizzo di inverter sui cuscinetti di motori da trazione asincroni," Ph.D. Dissertation, Dept. of Electrical and Computer Eng., University of Salerno, Italy, 2006 (in Italian).
23. Miano, G. and A. Maffucci, *Transmission Lines and Lumped Circuits: Fundamentals and Applications*, Academic Press Inc., 2001.
24. Beneduce, L., G. Costabile, B. de Vivo, L. Egiziano, S. Iovieno, A. Masucci, V. Tucci, and M. Vitelli, "An accurate evaluation of electric discharge machining bearings currents in inverter-driven induction motors," *European Conf. on Power Electronics and Applications (EPE 2007)*, 1–8, Aalborg, Denmark, 2007,
25. De Vivo, B., L. Egiziano, P. Lamberti, and V. Tucci, "Influence of circuit parameters on the electric discharge machining of the bearings of a PWM inverter driver motor," *International Symposium on Power Electronics, Electrical Drivers, Automation and Motion (SPEEDAM 2008)*, 1321–1324, Ischia, Italy, 2008.
26. Adabi, J., A. A. Boora, F. Zare, A. Nami, A. Ghosh, and F. Blaabjerg, "Common-mode voltage reduction in a motor drive system with a power factor correction," *IEEE Trans. on Power Electronics*, Vol. 5, No. 3, 366–375, 2012.
27. Busse, D., J. Erdman, R. J. Kerkman, D. Schlegel, and G. Skibinski, "Bearing currents and their relationship to PWM drives," *IEEE Trans. on Power Electronics*, Vol. 12, No. 2, 243–252, 1997.
28. Muetze, A., J. Tamminen, and J. Ahola, "Influence of motor operating parameters on discharge bearing current activity," *IEEE Trans. on Industry Applications*, Vol. 47, No. 4, 2011.